sciendo

Nordic Concrete Federation

ISSN online 2545-2819
ISSN print 0800-6377

DOI: 10.2478/ncr-2019-0091

Received: March 15, 2018
Revision received: March 15, 2019
Accepted: June 18, 2019

A Refined Model for Predicting Concrete-Related Failure Load of Tension Loaded Cast-in-Place Headed Anchors in Uncracked Concrete

Rasoul Nilforoush
Ph.D., Associate senior lecturer
Div. of Structural and Fire Engineering
Luleå University of Technology, LTU
SE-971 87 Luleå, Sweden.
Email: rasoul.nilforoush@ltu.se

ABSTRACT

Current theoretical models for predicting the concrete cone breakout capacity of tension loaded headed anchors do not consider the influence of member thickness, size of anchor head, and orthogonal surface reinforcement. In the present study, the influence of the aforementioned parameters was studied both numerically and experimentally. Both the numerical and experimental results showed that the tensile resistance of headed anchors increases by increasing the member thickness or if orthogonal surface reinforcement is present. In addition, the anchorage capacity further increases with increase of the anchor head size.

The current model for predicting the concrete cone failure load of tension loaded headed anchors were refined and extended by incorporating three modification factors to account for the influence of the member thickness, size of anchor head, and orthogonal surface reinforcement. The accuracy of the proposed model was verified based on the results of 124 tests on single headed anchors from literature.

Keywords: Concrete Cone Breakout, Concrete Splitting, Anchor Bolt, Headed Anchor, Fastening System, Member Thickness, Anchor Head Size, Surface Reinforcement.

1. INTRODUCTION

Fasteners of different kinds, including cast-in-place and post-installed anchors, are often used to anchor loads in concrete structures. An overview of various anchorage systems is given in Eligehausen et al. [1]. The cast-in-place anchors have been used ever since reinforced concrete was introduced around 1900. The post-installed anchors started to be used in the 1960s with the advances in drilling technology of concrete structures. Over the past few decades, numerous experimental and numerical studies were carried out on anchors of different kinds which led to the development of various theoretical and empirical models for designing anchorage systems to concrete. The capacity and performance of anchors were studied under particular test setups, limited boundary conditions, and certain loading circumstances. The development of such models involved many limitations and uncertainties and, hence, various simplifying assumptions were adopted. For instance, it is assumed that the thickness of concrete member, size of anchor head, and presence of orthogonal surface reinforcement have negligible influence on the tensile resistance of anchors.
In a sustainable society, buildings and structures must, from time to time, be adjusted to meet new demands. The capacity and/or service life of structures typically must be increased to comply with the new requirements, and this increase requires upgrading of both the structural components and the structural connections. Therefore, the structural connections can also be subjected to an increased service load or needed for extended service life. From the structural point of view, the adequacy of existing fastenings for the intended increased load or service life must be determined, and inadequate fastenings must either be replaced or upgraded. On the other hand, the current design methods for fastening systems are generally believed to be conservative. However, it is not very clear to what extent they are conservative. As the development of such models involved many limitations and uncertainties, their reliability should be evaluated particularly for other possible geometrical, loading, and boundary conditions than those considered previously.

The overall objective of the research presented in this paper is to form a background for developing improved methods for the design and assessment of cast-in-place headed anchors. The research scope is limited to single headed anchors under tension loads in uncracked concrete. As tension loaded headed anchors often fail via concrete cone breakout or concrete splitting/bending, the research focus is exclusively on these failure modes. The anchorage failure load in these cases depends strongly on the fracture properties of concrete, the geometry of concrete component, the amount and configuration of reinforcements in the anchoring zone, the type and magnitude of load on the anchor, and the position of anchor in respect to concrete free edges and adjacent anchors. In the present paper, the influences of member thickness, size of anchor head, and amount of orthogonal surface reinforcement on the capacity and performance of headed anchors are evaluated both numerically and experimentally.

2. BACKGROUND

The literature contains numerous analytical and theoretical approaches, based on various assumptions, for calculating the concrete cone breakout. The first theoretical model proposed for the concrete cone breakout failure was the 45-degree cone model, which was incorporated into ACI 349 [2]. This model assumes a cone angle of 45° with respect to concrete surface and constant tensile stress of ($f_{ct}= 0.3\sqrt{f_{cc}}$ N/mm^2) acting over the projected cone surface (see Fig. 1). Based on this model, the tensile breakout capacity of a single anchor is calculated as follows:

$$N_{\mathrm{u,m}} = 0.3\sqrt{f_{\mathrm{cc}}}\,\pi \cdot h_{\mathrm{ef}}^{2.0} \cdot \left(1 + \frac{d_{\mathrm{h}}}{h_{\mathrm{ef}}}\right) \tag{1}$$

where $N_{\mathrm{u,m}}$ is the mean concrete cone breakout failure load of a single anchor unaffected by concrete member edge/s and adjacent anchor/s [N], f_{cc} is the concrete cube compressive strength [N/mm^2], h_{ef} is the anchor embedment depth [mm], and d_{h} is the diameter of anchor head [mm].

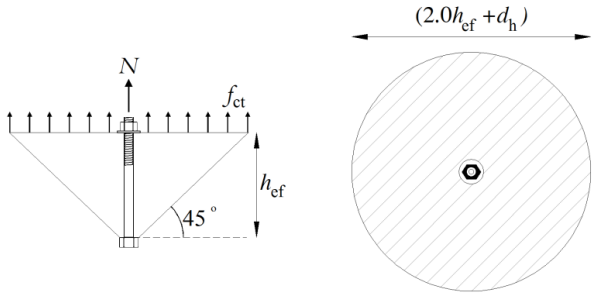

Figure 1 – Shape of concrete cone failure and the projected cone surface per 45-degree cone model [1].

This model was derived based on the results of pullout tests on headed anchors with a limited range of embedment depths (i.e. h_{ef} up to 150 mm) and therefore it does not account for a so-called size effect. The size effect on anchorage capacity exists because, at the ultimate load, the average tensile stress over the fracture surface decreases as the fracture area increases [1]. Moreover, subsequent experimental observations revealed that the slope of concrete cone surface is not constant over the embedment depth, which varies between 30° and 40° and is on average about 35° [1]. Therefore, Eq. (1) tends to overestimate the capacity of deep anchors because the assumptions of the constant tensile stress over the projected fracture surface and the cone angle of 45° deviate significantly from reality.

Fuchs et al. [3] later analyzed experimental results from a large database of European and American tests on various anchors at different embedment depths, and proposed a user-friendly method known as the Concrete Capacity (CC) method (i.e., known as Concrete Capacity Design CCD in the US). The CC method is an empirical model which takes the concrete's size effect into account. According to the CC method, the concrete cone failure load of a single cast-in-place anchor is estimated by assuming a concrete cone angle of ~35^0 with respect to the concrete surface. This assumption was reasonably supported by widespread observations that the horizontal extent of the concrete cone fracture on the surface of the concrete component is around $3.0 \cdot h_{\mathrm{ef}}$ (see Fig. 2).

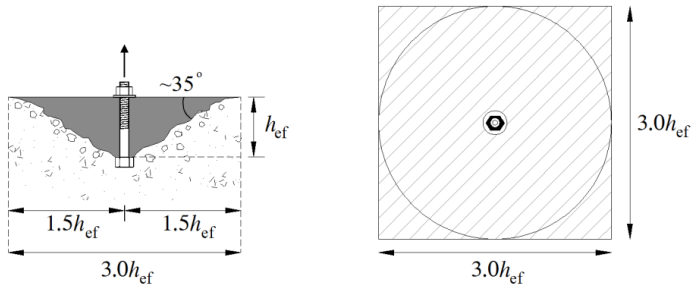

Figure 2 – Shape of concrete cone failure and the idealized cone surface per CC method [3].

The general form of the CC method for estimating the concrete cone failure load of a single anchor in uncracked concrete is as follows:

$$N_{u,m} = k_1 f_c^{0.5} \cdot k_2 h_{ef}^2 \cdot k_3 h_{ef}^{-0.5} = K\sqrt{f_c}\, h_{ef}^{1.5} \quad (2)$$

where f_c is the concrete cylinder compressive strength [N/mm^2], k_1, k_2 and k_3 are calibration factors; K is an empirical factor ($K= k_1 \cdot k_2 \cdot k_3$) which has a dimensional unit of [N$^{0.5}$/mm$^{0.5}$]; $k_1 f_c^{0.5}$ represents the nominal concrete tensile stress at failure over a failure area given by $k_2 h_{ef}^2$; and $k_3 h_{ef}^{-0.5}$ accounts for the concrete size effect which was derived based on the fracture mechanics theory.

Based on evaluation of results of various tests, Fuchs et al. [3] proposed the following equation for concrete cone failure of a single-headed anchor under concentric tension that is positioned far from the concrete free edge/s and adjacent anchor/s in an uncracked concrete member:

$$N_{u,m} = 16.8\sqrt{f_c}\, h_{ef}^{1.5} \quad (3)$$

According to Eligehausen et al. [1] and Fuchs et al. [3], the concrete cube and cylinder strengths are related as ($f_c \approx 0.84 \cdot f_{cc}$). Therefore, if the concrete cube compressive strength (f_{cc}) is given instead of the concrete cylinder compressive strength (f_c), the leading coefficient of Eq. (3) is 15.5 rather than 16.8. Equation 3 was incorporated into several design-oriented documents and standards in Europe such as the CEB Design Guide [4] and CEN/TS 1992-4 [5], internationally in the *fib* Bulletin 58 [6], and in several US design standards (e.g., ACI 349 [7] and ACI 318 [8]).

Based on the CC method, the mean tensile breakout capacity of a single anchor is proportional to $h_{ef}^{1.5}$. However, subsequent numerical and experimental studies [9-13] showed that Eq. (3) may result in conservative capacities for deep embedment depths. For deep anchors (where $h_{ef} \geq 280$ mm), American standards [7,8] allow the use of a modified CC method as below:

$$N_{u,m} = 16.8\sqrt{f_c}\, h_{ef}^{1.5} \quad \text{for } h_{ef} < 280 \text{ mm} \quad (4.a)$$

$$N_{u,m} = 6.585\sqrt{f_c}\, h_{ef}^{5/3} \quad \text{for } 280 \text{ mm} \leq h_{ef} \leq 635 \text{ mm} \quad (4.b)$$

The modified CC method uses an exponent of 5/3 (=1.667) rather than 1.5 for the effective embedment depth of deep anchors ($h_{ef} \geq 280$ mm) and appropriately changes the leading coefficient of the CC method. Equations (3) and (4) were developed based on the results of numerous pullout tests on headed anchors at various embedment depths. The concrete cylinder compressive strength was in the range of 13 to 50 [N/mm^2]. The ratios of measured concrete cone breakout capacities to the values predicted by the CC method ($N_{test}/N_{CC\ method}$) as a function of anchor embedment depth are presented in Fig. (3a). The figure shows the experimental results of 320 pullout tests on single-headed anchors reported in the literature [10-12]. The tested anchors had various head sizes and were embedded in un-reinforced and reinforced concrete members of various thicknesses, leading to a wide scatter in the obtained capacities. As the tested headed anchors had different head sizes, the concrete in the vicinity of the anchor heads experienced various bearing pressures. According to ACI 349 [7] and ACI 318 [8], to prevent a pullout failure and ensure a concrete cone breakout failure for cast-in-place headed anchors, the mean concrete pressure (σ_b) under the head of anchors in uncracked concrete is limited to ($15 \cdot f_c$). This indicates that, at anchor's peak load (N_u), a minimum bearing area of ($A_{b,min} = N_u/15 \cdot f_c$) is required to prevent a pullout failure and allow the formation of a concrete cone failure. Fig. (3b) presents the ratios of bearing areas of anchor heads to their corresponding minimum required bearing areas ($A_b/A_{b,min}$) as a function of anchor embedment depth, for the tested headed anchors (test data in Fig. 3(b) corresponds to those presented in Fig. (3a)).

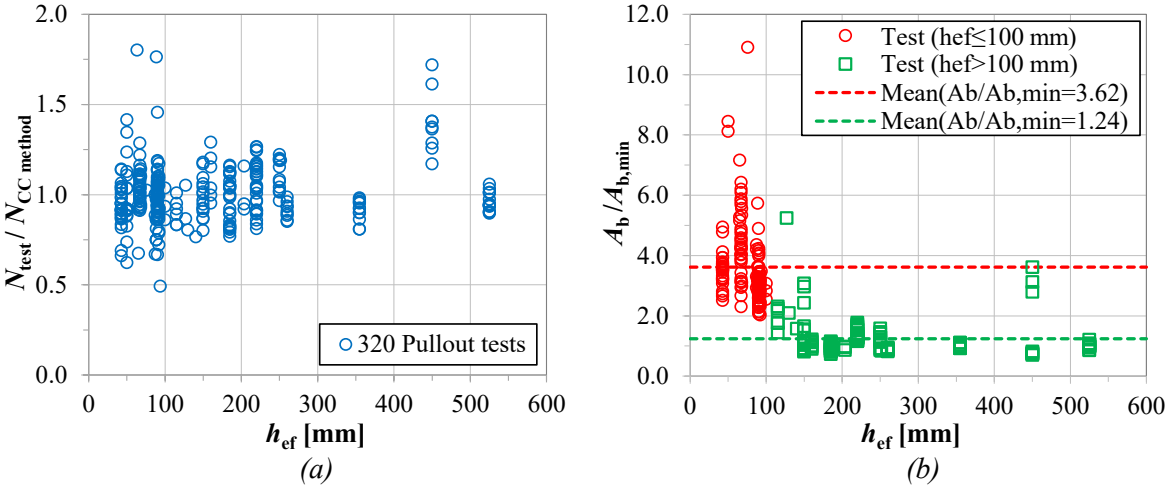

Figure 3 – (a) ratio of measured concrete cone failure loads to values predicted by CC-method (Eq. 3) as a function of anchor embedment depth for 320 pullout test from literature, and (b) ratio of bearing area of anchor heads to their minimum required bearing areas corresponding to concrete pressure of 15·f_c under anchors head at peak load as a function of anchor embedment depth.

As the figure shows, the bearing area of the tested anchors varied significantly from 0.7·$A_{b,min}$ to 10.9·$A_{b,min}$. For short anchors (h_{ef}≤100 mm), the mean ratio of the bearing area to the minimum bearing area (A_b/$A_{b,min.}$) is 3.62, while this ratio is only 1.24 (i.e. almost three times smaller) for deep anchors (h_{ef}>100 mm). This indicates that the CC method has not been developed systematically with respect to the size of anchor head, as the bearing area of the tested short and deep headed anchors varied significantly. The results presented in Fig. 3 show that the CC method may underestimate or overestimate the failure load of headed anchors if their head sizes differ appreciably from those of previously tested short and deep anchors.

In practice, headed anchors with various head sizes are often used in unreinforced or reinforced concrete members with different geometries. However, the CC method was developed based on the simplifying assumptions that the member thickness, surface reinforcement, and the size of anchor head have negligible effects on the tensile capacity of headed anchors. In addition to the uncertainties discussed above, and despite several recent experimental and numerical investigations into the capacity of cast-in-place headed anchors [9-11], the influence of the thickness of concrete component, presence of orthogonal surface reinforcement and the size of anchor head on the failure load of headed anchors is still unknown. In the present paper, systematic numerical and experimental studies are carried out to evaluate the influence of each parameter on the anchorage capacity and performance. The result of this study can provide a basis for developing improved methods of the design and assessment of headed anchors with various head sizes in unreinforced or reinforced concrete members of different geometries.

3. NUMERICAL STUDIES

For the purpose of this research, extensive three-dimensional (3D) FE numerical analyses were carried out through the FE program MASA (MAcroscopic Space Analysis). This program was previously developed at the Institute of Construction Materials in University of Stuttgart, Germany. For modeling the nonlinear behavior of concrete, the employed constitutive material model was based on the microplane constitutive law in the framework of the smeared crack approach. Detailed discussions of the features and various aspects related to the Microplane model can be found in Ožbolt et al. [14]. The behavior of steel in the anchor was considered as linear

elastic. For pre- and post-processing analysis, the commercial program FEMAP® was used. In general, the classical smeared fracture analysis of quasi-brittle materials leads to mesh-dependent results. To avoid mesh size sensitivity, the total energy consumption capacity of a model due to cracking should be independent of its element size. In this study, the crack band theory proposed by Bažant and Oh [15] was employed in all analyses, in which the constitutive law was related to the element size such that the concrete fracture energy G_f was independent of the elements' sizes.

3.1 Matrix and geometry of numerical models

To systematically evaluate the influence of member thickness, anchor head size and orthogonal surface reinforcement on the tensile breakout capacity of headed anchors, three simulation series were carried out (see the matrix of numerical studies in Table 1). In series (a), headed anchors at various embedment depths (h_{ef}=50–500 mm) were simulated in unreinforced concrete members of various thicknesses (H=1.5-5.0h_{ef}). In series (b), headed anchors at various embedment depths (h_{ef}=50–500 mm) were considered to have various head sizes (i.e., small, medium and large heads). For this simulation series, all concrete members were unreinforced, and the member thickness was (H=3.0h_{ef}). In series (c), headed anchors at various embedment depths (h_{ef}=50–300 mm) were simulated in reinforced concrete slabs of various thicknesses (H=1.5-3.0h_{ef}). For this case, the concrete slabs were orthogonally reinforced and considered to have small and large reinforcement ratios to also evaluate the influence of reinforcement amount on the anchorage capacity and performance. The ratio of the top or bottom reinforcements in each direction for the small-content was approximately 0.3%, while for the large-content was larger than 0.5%. The total number of simulations in each series is given in Table 1. Each anchor embedment depth was simulated with each member height (in series a), with each anchor head size (in series b), and with each member height and reinforcement-content (in series c).

Table 1 – Matrix of numerical studies

Series	Total number of models	h_{ef} [mm]	Head size	Member height H	Bar condition
(a) Member thickness	30	50 100 200 300 500	Medium	$1.5\cdot h_{ef}$ $2.0\cdot h_{ef}$ $2.5\cdot h_{ef}$ $3.0\cdot h_{ef}$ $4.0\cdot h_{ef}$ $5.0\cdot h_{ef}$	Un-reinforced
(b) Anchor head size	15	50 100 200 300 500	Small Medium Large	$3.0\cdot h_{ef}$	Un-reinforced
(c) Reinforcement amount	24	50 100 200 300	Medium	$1.5\cdot h_{ef}$ $2.0\cdot h_{ef}$ $3.0\cdot h_{ef}$	Small-reinforcement content ($\rho\approx0.3\%$) & Large- reinforcement content ($\rho>0.5\%$)

The typical geometry of the FE models is shown in Fig. 4. In all FE models, one single anchor was simulated in the center of a rectangular concrete member. For all simulation series, the

geometry of the concrete members was defined systematically so that the length (L) and width (W) of the components, for all embedment depths of anchors, are proportional to the anchor embedment depth (L=W=6.0·h_{ef}). For simulating the anchor pullout loading, a line circular support with a span of (L_{sup}=4.0·h_{ef}) was considered for all numerical models to permit an unrestricted formation of a concrete cone fracture.

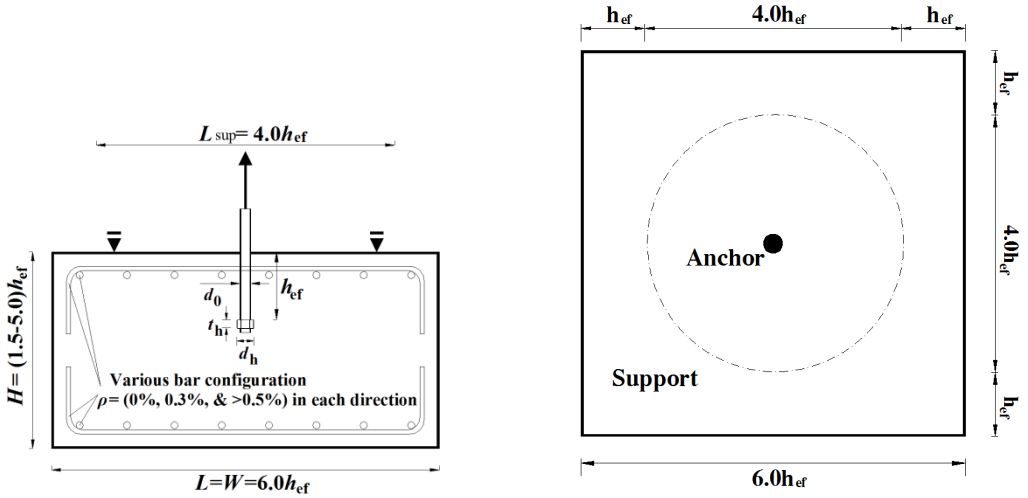

Figure 4 – Typical geometry of FE numerical models: (a) side view, and (b) top view.

The dimensions of anchors, including the embedment depth h_{ef}, shaft diameter d_0, head diameter d_h, and head thickness t_h for the studied anchors are summarized in Table 2. For series (b), the diameter of the anchors' head was set so that the concrete pressure under anchor head at anchors' peak load would be almost constant for all investigated embedment depths of anchors. The peak load for all anchors was predicted using the CC method (Eq. 3). The concrete pressure under anchor head at peak load (σ_b) for the simulated small-, medium- and large-headed anchors were approximately 20· f_c, 11·f_c, and 4·f_c, respectively.

Table 2 – Dimensions of simulated headed anchors at various embedment depths.

h_{ef} [mm]	d_0 [mm]	t_h [mm]	$d_{h,small}$ [mm]	$d_{h,medium}$ [mm]	$d_{h,large}$ [mm]
50	10	10	13.0	16.0	21.0
100	16	15	21.4	25.0	35.0
200	30	25	38.4	45.0	62.0
300	40	35	51.5	60.0	83.0
500	60	45	76.0	85.0	122.0

3.2 FE discretization and simulation procedure

The typical discretized 3D FE models for headed anchors in unreinforced and reinforced concrete members are shown in Fig. 5. Due to the symmetrical geometry of the numerical models, only one-quarter of the specimens were simulated to save the CPU and computational time. This has been done by introducing double symmetry boundary conditions along the symmetrical axes. In all models, the concrete and anchor were discretized with tetrahedral and hexahedral solid finite elements, respectively. The size of FE elements was defined as approximately 30-50 mm at the concrete free edges (depending on the global size of the FE model), whereas they are refined to

approximately 5-10 mm in the vicinity of the anchor. The vertical support for anchor pullout loading was defined by constraining the support nodes in the loading direction.

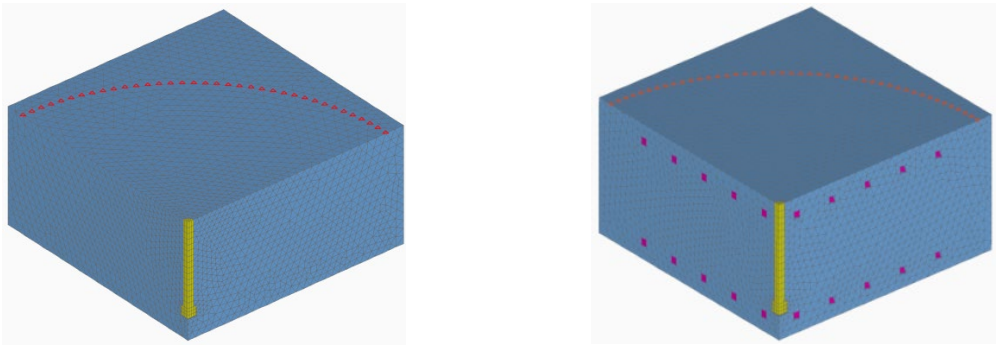

(a) *(b)*

Figure 5 – Typical discretized 3D FE models for anchors cast in: (a) unreinforced concrete, and (b) reinforced concrete.

The reinforcement at the top and bottom surface of the reinforced slabs were modeled using a 3D smeared approach in a way that they were assumed to be smeared inside a row of concrete elements (see Fig. 6). The 3D smeared reinforcements were discretized using eight-node solid elements with equivalent material properties defined as weighted average of the properties of concrete and reinforcement. The equivalent properties of the 3D smeared reinforcements were defined using the expression given in Fig. 6. In simulations, the equivalent properties of smeared reinforcements were defined using the uniaxial elasto-plastic stress-strain relationship with steel strain hardening. The hardening modulus of the 3D smeared reinforcement $E_{s,h}$ was considered as 1% of the equivalent modulus of elasticity of the 3D smeared reinforcement. The 3D von Mises yield criterion was used for analyzing the smeared reinforcement.

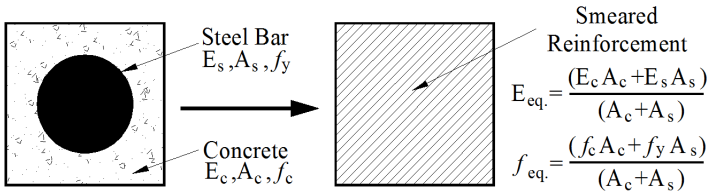

Figure 6 – Concept of 3D smeared reinforcement. .

Before creating all FE models, several FE models were initially calibrated and verified against the results of a previous experimental study performed by Nilsson et al. [11]. A series of parametric studies were also carried out to evaluate the influence of concrete material properties (i.e., concrete tensile strength f_{ct} and compressive strength f_c, concrete young modulus E_c, concrete fracture energy G_f, and concrete Poisson's ratio υ_c), boundary conditions (i.e., full model and one-quarter model), size of mesh elements, and loading rate on the numerical results. For a complete description of the FE verification procedure and parametric studies see Nilforoush [16].

The material properties of concrete and steel in the anchor and reinforcement, in all FE analyses, were identical to the material properties of the initially calibrated and verified FE models.

The concrete properties used for all FE models were as follows: uniaxial compressive strength f_c=28 [N/mm^2], uniaxial tensile strength $f_{c,t}$=2.2 [N/mm^2], Young's modulus E_c=35000 [N/mm^2], fracture energy G_f=70 [N/m], and Poisson's ratio υ_c=0.18. The mechanical properties of steel reinforcement were considered as follows: modulus of elasticity E_s=210 000 [N/mm^2], Poisson's ratio υ_s=0.33, yield strength $f_{y,s}$ =500 [N/mm^2], and ultimate strength $f_{u,s}$=600 [N/mm^2]. The

behavior of steel in the anchor was assumed to be linear elastic with Young's modulus E_s=210000 [N/mm^2] and Poisson's ratio υ_s=0.33. The anchor pullout load was simulated as displacement controlled by defining incremental deformations with a displacement-increment rate of 0.05 mm/increment on the top of anchor shaft.

Contact between the concrete and the steel anchor was assumed to exist only at the top surface of the anchor head. In addition, a very thin gap was defined between the concrete and the bottom surface of the anchor head. Moreover, a very thin interface layer which can only take up compressive stress was modeled between the anchor shaft and the concrete body, along the entire length of the anchor shaft. For the interface layer, no friction was considered between anchor shaft and concrete body as the tensile load on the anchor is mainly transferred by the anchor bearing head.

4. EXPERIMENTAL STUDIES

4.1 Matrix and geometry of test specimens

A supplementary experimental study was carried out to clarify the influence of member thickness, size of anchor head, and orthogonal surface reinforcement on the anchorage capacity and performance. A total of nineteen headed anchors cast-in unreinforced and reinforced concrete slabs were tested under monotonic tensile loading. Like the numerical study, three test series were considered in which the testing parameters were the same as in the numerical study (see the matrix of experiments in Table 3). Headed anchors at only one size of embedment depth were tested (h_{ef}=220 mm). The number of test replicates for series (a) was three; while for series (b) and (c), they were two in each. Figure 7(a) shows the typical geometry of test specimens and tested headed anchors. In all test series, a single headed anchor was placed in the center of a rectangular concrete block. The length and width of concrete blocks for all specimens were identical (L=W=1300 mm), whereas their heights varied (H= 330, 440 and 660 mm). The member heights of 330, 440, and 660 mm correspond to 1.5h_{ef}, 2.0h_{ef}, and 3.0h_{ef} , respectively.

Table 3 – Matrix of experiments

Series	h_{ef} [mm]	Head size	Member height [mm]	Bar configuration
a) Member thickness	220	Medium	330 440 660	Un-reinforced
(b) Anchor head size	220	Small Medium Large	660	Un-reinforced
(c) Surface reinforcement	220	Medium	330 440 660	8Ø12#150 mm 8Ø16#150 mm 8Ø20#150 mm

The headed anchors were composed of standard threaded 36-mm-diameter rods with a round bearing head at the end. To prevent the steel failure of anchors, high-strength steel rods of grade 10.9 with a yield strength of f_{yk}=900 [N/mm^2] and an ultimate strength of f_{uk}=1000 [N/mm^2] were used. To evaluate the influence of the size of anchor head, three different sizes of bearing head were tested (i.e., small, medium, and large). The geometry of headed anchors with small, medium and large heads is shown in Fig. 7(b). For the small- and medium-headed anchors, round nuts with diameters of d_h= 48 and 55 mm, respectively, were affixed to the end of threaded rods. For large-

headed anchors, a thick circular steel plate with diameter d_h= 90 mm was tapped and fastened to the end of the threaded rods. A standard hex nut was also tightened underneath of the steel plate to ensure that the plate remains in place during anchor pullout loading (see Fig. 7b). All threaded rods were covered with 2-mm-thick plastic tubes. These tubes were used to prevent friction and adhesion between the anchor shaft and concrete body, thereby ensuring the transfer of the entire load through the anchor bearing head.

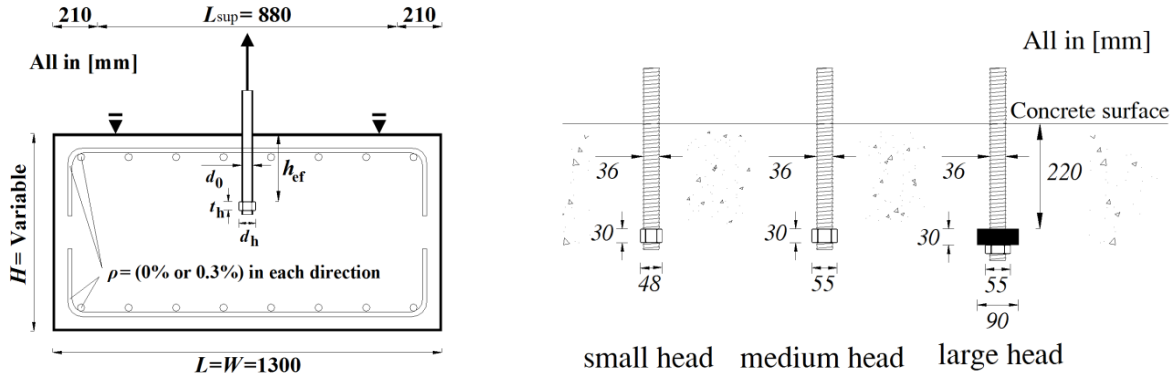

Figure 7 – Typical geometry of (a) test specimens, and (b) tested headed anchors with various head size.

The concrete blocks were cast using a ready-mix normal-weight concrete of grade C30/37 made of crushed aggregates. The mix proportion of concrete is given in Table 4. The cube compressive strength and tensile splitting strength of concrete at the time of anchor pullout loading were measured in accordance with EN 12390-3 [17] and EN 12390-6 [18], respectively. The measured cube compressive and tensile splitting strengths were f_{cc}=39.5 [N/mm^2] and $f_{t,sp}$=3.2 [N/mm^2], respectively.

Table 4 – Mix proportion of tested concrete

Cement (kg/m^3)	380
Aggregate 0–4 mm (kg/m^3)	500
Aggregate 4–8 mm (kg/m^3)	450
Aggregate 8–16 mm (kg/m^3)	840
w/c	0.55

If the cylinder compressive strength of concrete f_c for tested specimens is equivalent to $0.85 \cdot f_{cc}$ and anchorage peak load is estimated using the CC method (Eq. 3), the average concrete pressure under anchor head at peak load (σ_b) for the tested small-, medium- and large-headed anchors would be $16.5 \cdot f_c$, $8.3 \cdot f_c$ and $1.8 \cdot f_c$, respectively.

The tested reinforced concrete slabs were designed to have a small reinforcement amount: a reinforcement ratio of ρ~0.3% was applied in each surface and direction. They had orthogonal surface reinforcement at 150 mm spacing at the top and the bottom of the concrete blocks. The concrete cover was in all directions 50 mm. The reinforcing bars were of a class B500B with a yield strength of f_{yk} of 500 [N/mm^2], according to the manufacturer's specifications.

4.2 Test setup and test procedure

The test setup and loading arrangement are shown in Fig. 8. The anchor pullout loading was carried out after the concrete had cured for ~60 days to exclude the influence of concrete strength

growth at the time of anchor pullout testing. For anchor tension loading, the vertical reaction was taken up by a stiff circular steel ring with a width of 100 mm and an inner diameter of L_{sup}= 880 mm (i.e., correspond to 4.0·h_{ef}). The anchor tension loading was displacement-controlled by applying incremental deformations on the top of the anchor shaft at a constant displacement rate of 1 mm/min. The load was applied by means of a 100-ton hollow cylinder hydraulic jack. The time-deformation relation was kept approximately linear for the entire test duration. The applied load was measured by a load cell placed on the top of the jack.

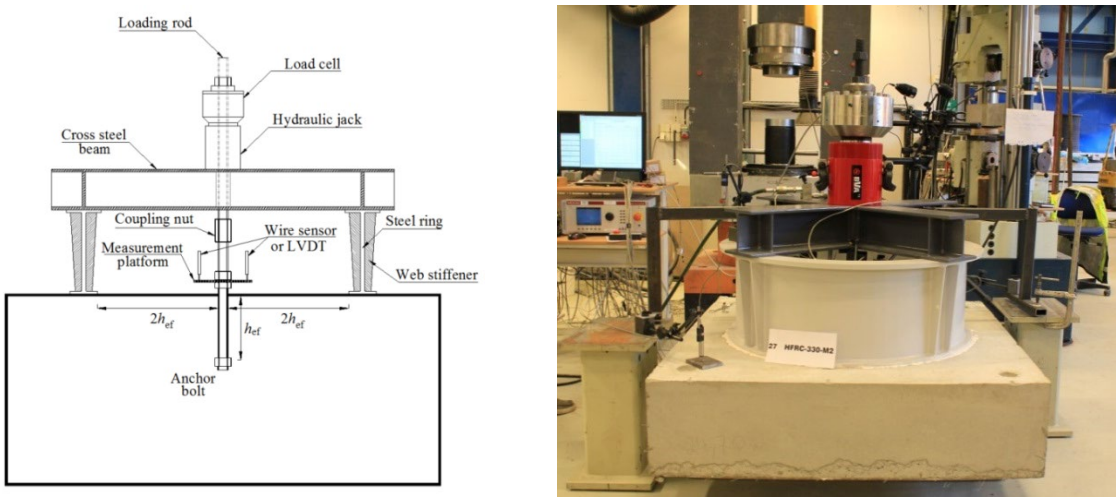

(a) *(b)*

Figure 8 – (a) Schematic view of the test setup, and (b) loading arrangement

The anchor displacement was measured relative to the solid ground rather than the concrete surface to measure the anchor displacement accurately even at post-peak loads. For this reason, a measurement platform fabricated from a square steel plate (150 × 150 mm) was secured perpendicular to the testing anchor, 50 mm above the concrete surface, using a hex nut above and another below the platform (see Fig. 8a). The surface of the platform served as the reference level for measuring the vertical displacement of anchor. The vertical displacement was measured by two linear variable differential transformers (LVDTs) installed symmetrically at two side of the anchor. The LVDTs measured the displacement of the anchors relative to two rigid points outside the concrete block, on the solid ground, by means of two rigid frames (see Fig. 8b). The frames were supported from outside the blocks and contact with other structural members and testing equipment (which could have produced inaccurate displacement readings) was prevented. The anchor displacement was taken as the average of the two LVDTs. It should be noted that the measured displacement values also include the bending deformation of the tested concrete slabs.

5. RESULTS AND DISCUSSIONS

Due to large number of numerical results, only numerical results of headed anchors at 200 mm embedment depth, in all simulation series, are presented here. For detailed numerical results at other embedment depths see Nilforoush et al. [19,20]. In addition, the results of tested headed anchors at 220 mm embedment depth are presented in the following. In section 6, the numerical and experimental results at all embedment depths are used to evaluate the reliability of the CC method in predicting the concrete cone failure load of cast-in-place headed anchors.

5.1 Influence of member thickness (series a)

The numerical and experimental results of headed anchors in unreinforced concrete members of various thicknesses (i.e., series a) showed that the tensile resistance of anchors increases up to 20% with increasing the member thickness. The numerically obtained load-displacement curves and post-peak crack patterns for headed anchors at h_{ef}=200 mm in unreinforced concrete members of various thicknesses are shown in Figs. 9(a) and 9(b), respectively. The anchorage is governed by concrete bending/splitting cracks in thin unreinforced concrete members (H<2.0·h_{ef}), while it is governed by concrete cone breakout in thicker members (H≥2.0·h_{ef}). The simulation results of series (a) indicate that there is a transition zone where the failure mode changes. This transition occurs at a relative member thickness of H/h_{ef}=2.0 for all anchor embedment depths investigated. The numerical findings are in very good agreement with the experimental results; see the load-displacement curves and crack patterns obtained at experiments in Figs. 10(a) and 10(b), respectively.

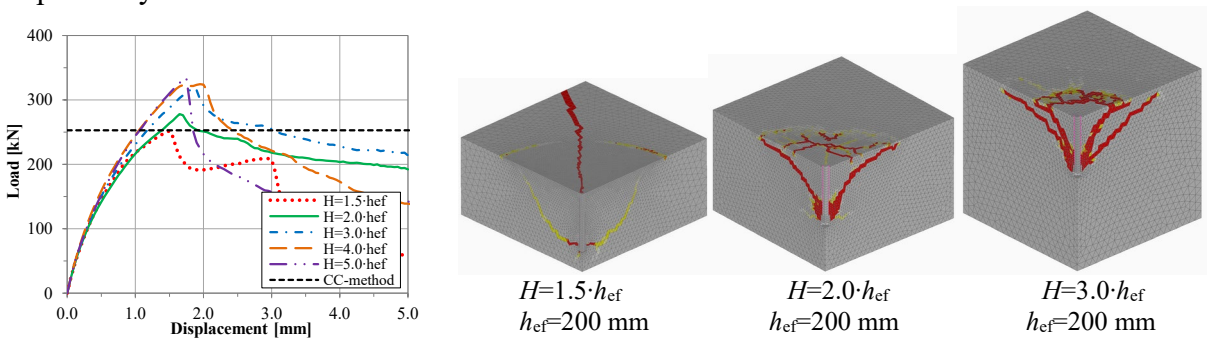

(a) *(b)*

Figure 9 – (a) load-displacement curves, and (b) crack patterns obtained for the simulated anchors in unreinforced concrete members of various thicknesses, f_c=28 [N/mm^2] and f_t=2.2 [N/mm^2].

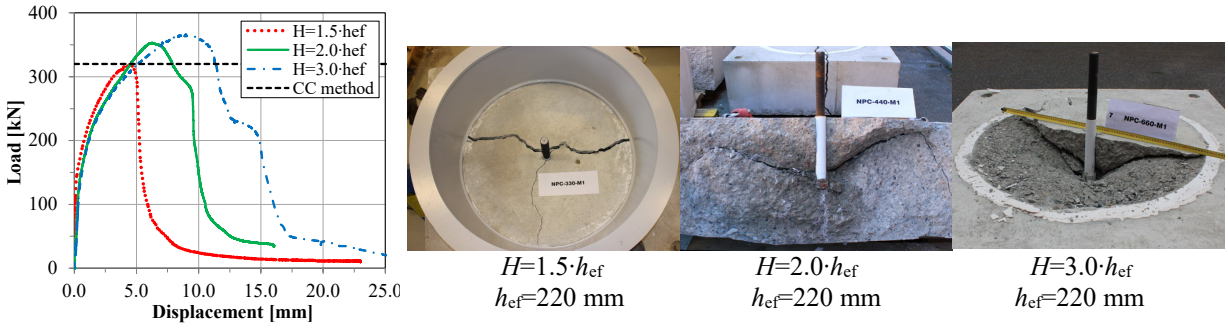

(a) *(b)*

Figure 10 – (a) load-displacement curves and (b) failure patterns of the tested anchors in unreinforced concrete members of various thicknesses, f_{cc}=39.5 [N/mm^2] and $f_{t,sp}$=3.2 [N/mm^2].

The concrete compressive and tensile strength at the numerical and experimental studies were different. Also note that the presented numerical results are for headed anchors with 200 mm embedment depth, while the test results are for headed anchors at 220 mm embedment depth. The load-displacement curves in Figs. 9(a) and 10(a) also show the failure load predicted by the CC method (Eq. 3) for the respective concrete strengths and embedment depths of anchors. As can be seen, the tendencies observed in the numerical analysis regarding increasing failure load and change of failure mode by increasing member thickness are fully supported by the experimental results. It should be noted that the anchor displacements, in all experiments, were generally larger than those in the simulations. This discrepancy is attributed to two reasons: (*a*) at experiments, the concrete in the vicinity of anchor head was locally damaged which resulted in a gradual slip

of the tested anchors and consequently an increased anchor displacement. However, this local damage of concrete cannot be accounted for in the macroscopic finite element analysis. (*b*) The displacements at tests were measured with respect to the solid ground rather than the concrete surface, to capture the load-displacement relationship of the tested anchors at post peak loads. Therefore, the measured displacements at tests include also the bending deformation of the tested concrete components, which is not accounted for in the simulations.

5.2 Influence of size of the anchor head (series b)

The numerical and experimental results of headed anchors with various head sizes (i.e., series b) showed that the anchorage capacity and stiffness increases by increasing the head size. However, the post-peak anchorage behavior became more brittle by increasing the head size. The numerically obtained load-displacement curves and the post-peak crack patterns for headed anchors at 200 mm embedment depth with various head sizes (i.e., small, medium and large) are shown in Figs. 11(a) and 11(b), respectively.

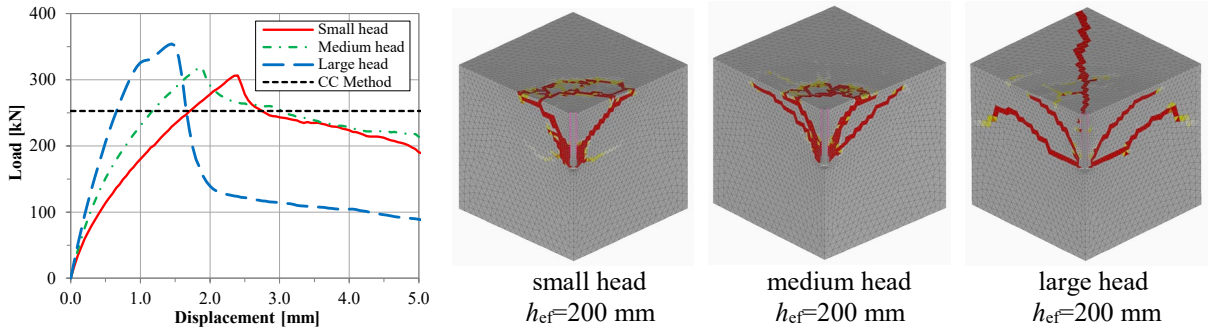

Figure 11 – (a) load-displacement curves, and (b) crack patterns obtained for the simulated anchors with various head sizes, f_c=28 [N/mm^2] and f_t=2.2 [N/mm^2].

As can be seen, irrespective of the head size, the anchorage is governed by concrete cone breakout failure as the anchors are placed in relatively thick components. However, the average concrete cone angle, with respect to the concrete surface, decreases with increase of the head size. It can also be seen that the diameter of the cone fracture at the concrete surface increases by increasing the head size. These findings are strongly supported by the experimental results: see the load-displacement curves and crack patterns obtained in tests in Figs. 12(a) and 12(b), respectively.

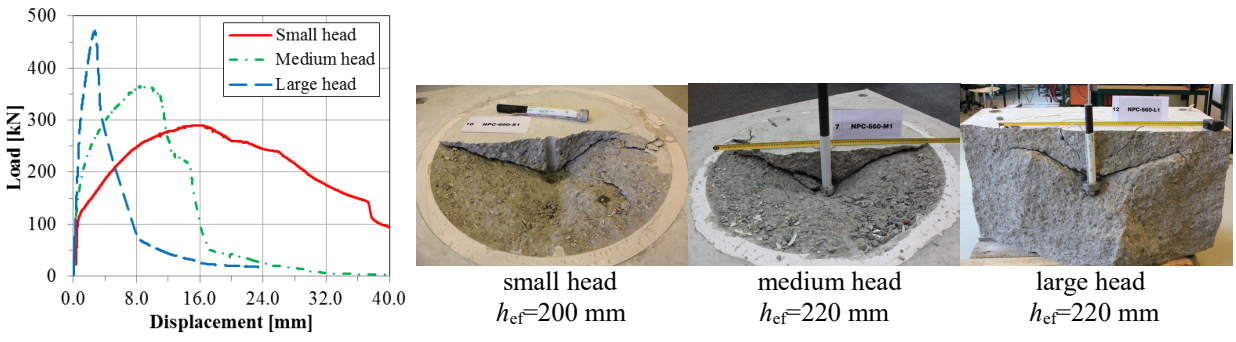

Figure 12 – (a) load-displacement curves, and (b) crack patterns obtained for the tested anchors with various head sizes, f_{cc}=39.5 [N/mm^2] and $f_{t,sp}$=3.2 [N/mm^2].

In all experiments, it was intended to position the anchors at an embedment depth of 220 mm; however, after casting the concrete slabs, an embedment depth of 200 mm was realized for the specimens with the small-headed anchors. Therefore, the capacity of the tested small-headed anchors would be slightly higher if they had the same embedment depth as the tested medium- and large-headed anchors. If the measured capacity of small-headed anchors at tests is normalized to the effective embedment depth of h_{ef}=220 mm using a normalizing factor of $(220/h_{ef,test})^{1.5}$, then the experimental results show an increased rate of approximately 34% with increasing the head size. The results of simulated headed anchors at various embedment depths, however, showed a lower increase rate: the increase rate was up to 16% with increasing the head size. This discrepancy might be related to the fact that the bearing area of tested large-headed anchors was relatively larger than that of the simulated large-headed anchors. In fact, the concrete pressure under the head of the tested large-headed anchors (σ_b=1.8·f_c) was less than half of the concrete pressure under the head of the simulated large-headed anchors (σ_b=4·f_c).

Moreover, as figures 11(b) and 12(b) show for the simulated and tested large-headed anchors, the propagation of concrete cone cracks, at post-peak loads, is hindered by the concrete confined zone under the vertical support. This resulted in transitioning the failure mode to concrete bending cracking at post-peak loads. As this transition of failure mode happened at post-peak loads, thus it did not seem to affect the anchorage capacity, however, affected the post-peak anchorage behavior. This change of failure mode at post-peak loads can explain the brittle post-peak behavior of the large-headed anchors; see Figs. 11(a) and 12(a).

5.3 Influence of surface reinforcement (series c)

The numerical and experimental results of headed anchors in reinforced concrete members (i.e., series c) showed that the anchorage capacity and post-peak resistance increase if a small amount of orthogonal surface reinforcement is present (i.e. ρ≈0.3% in each direction). The comparison of numerically obtained load-displacement curves of headed anchors at 200 mm embedment depth in unreinforced and reinforced concrete members of various thicknesses are shown in Fig. 13. In this figure, from the left to the right, the member thickness increases from 1.5 to 3.0 times the anchor embedment depth.

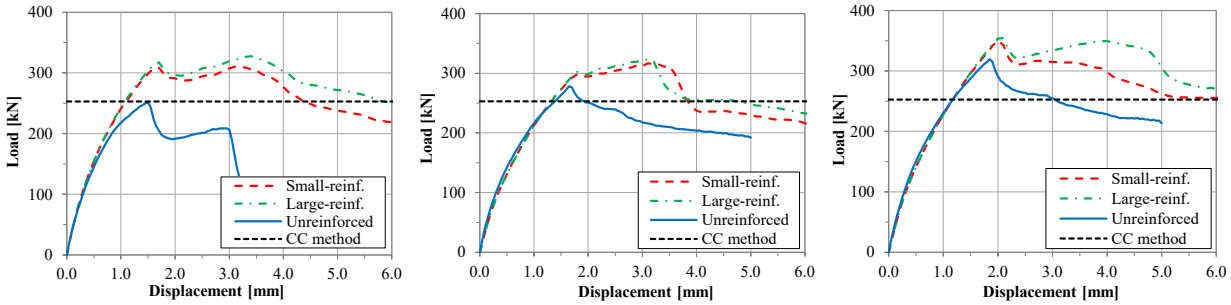

(a) $H=1.5h_{ef}$, h_{ef}=200 mm *(b) $H=2.0h_{ef}$, h_{ef}=200 mm* *(c) $H=3.0h_{ef}$, h_{ef}=200 mm*

Figure 13 – Comparison of load-displacement curves of the simulated headed anchors in unreinforced and reinforced concrete members of various thicknesses, f_c=28 [N/mm^2] and f_t=2.2 [N/mm^2].

As the figure shows, the applied orthogonal surface reinforcement has a more favorable effect on the anchorage capacity of headed anchors in the thin members than those in the thick members. This is due to the fact that the global bending stiffness of concrete members increases by applying

orthogonal surface reinforcement which prevents the formation of bending/splitting cracks in thin members, thereby allowing concrete cone cracks to develop and govern the anchorage failure.

Fig. 13 further shows that the large-reinforcement content (i.e. ρ>0.5% in each direction) did not improve the anchorage capacity and performance any further than the small-reinforcement content (ρ≈0.3%). The same tendencies were observed for all simulated embedment depths of anchors. The load-displacement curves for the tested headed anchors in reinforced concrete slabs of various thicknesses are shown in Fig. 14. As can be seen, the experimental results confirm the tendencies observed in the numerical study.

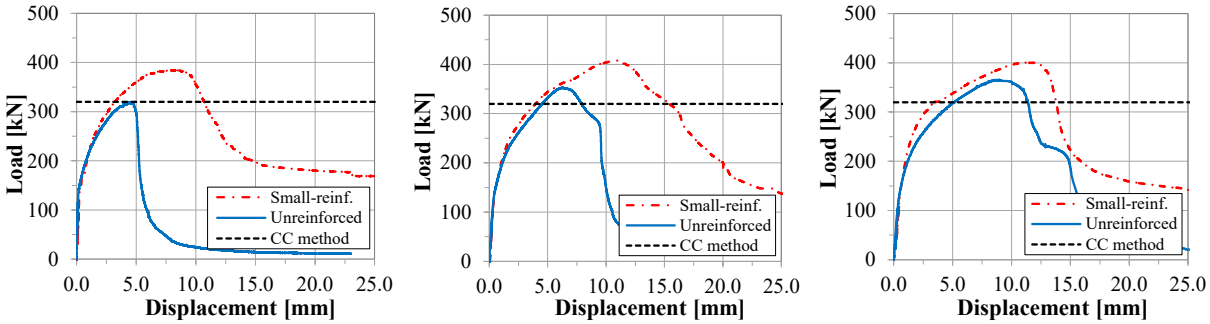

(a) $H=1.5h_{ef}$ h_{ef}=220 mm *(b) $H=2.0h_{ef}$ h_{ef}=220 mm* *(c) $H=3.0h_{ef}$ h_{ef}=220 mm*

Figure 14 – Comparison of load-displacement curves of the tested anchors in unreinforced and reinforced concrete members of various thicknesses, f_{cc}=39.5 [N/mm^2] and $f_{t,sp}$=3.2 [N/mm^2].

The crack patterns obtained for headed anchors in reinforced concrete members of various thicknesses at simulations and tests are shown in Figs. 15 and 16, respectively. The failure of all simulated and tested headed anchors in reinforced concrete members was concrete cone breakout. In fact, the observed concrete bending/splitting failure in the thin unreinforced concrete is prevented by a small amount of orthogonal surface reinforcement.

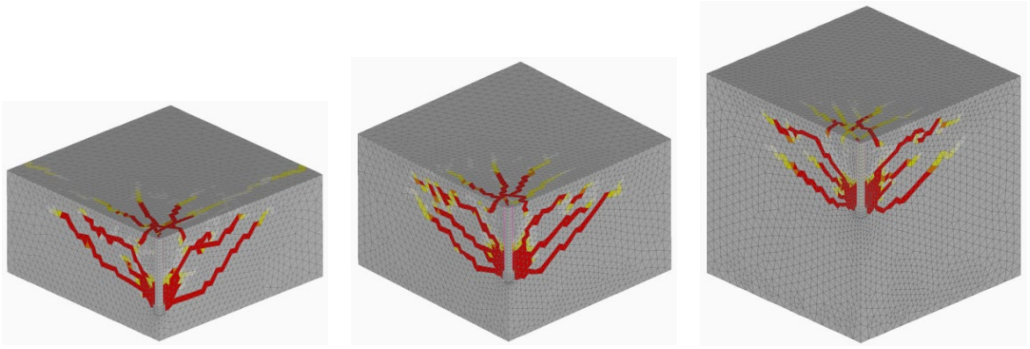

(a) $H=1.5h_{ef}$ h_{ef}=200 mm *(b) $H=2.0h_{ef}$ h_{ef}=200 mm* *(c) $H=3.0h_{ef}$ h_{ef}=200 mm*

Figure 15 – Crack patterns of the simulated anchors in reinforced concrete members of various thicknesses.

(a) $H=1.5h_{ef}$ $h_{ef}=220$ mm *(b) $H=2.0h_{ef}$ $h_{ef}=220$ mm* *(c) $H=3.0h_{ef}$ $h_{ef}=220$ mm*

Figure 16 – Crack patterns at tests for anchors in reinforced concrete members of various thicknesses.

5.4 Influence of span of vertical support

To better understand if the geometry of concrete slab and the span of vertical support has an impact on the anchorage failure load and failure mode, additional analyses were carried out. For this reason, two headed anchors at 200 mm embedment depth with a medium head size were modeled in larger concrete slabs with a length and width of ($L=W=9.0h_{ef}$). In both analyses, the member height was identical ($H=2.0h_{ef}$), but the span of vertical support was different ($L_{sup}=4.0h_{ef}$ and $8.0h_{ef}$). Figure 17 shows the crack patterns obtained for the simulated headed anchors with small and large supports.

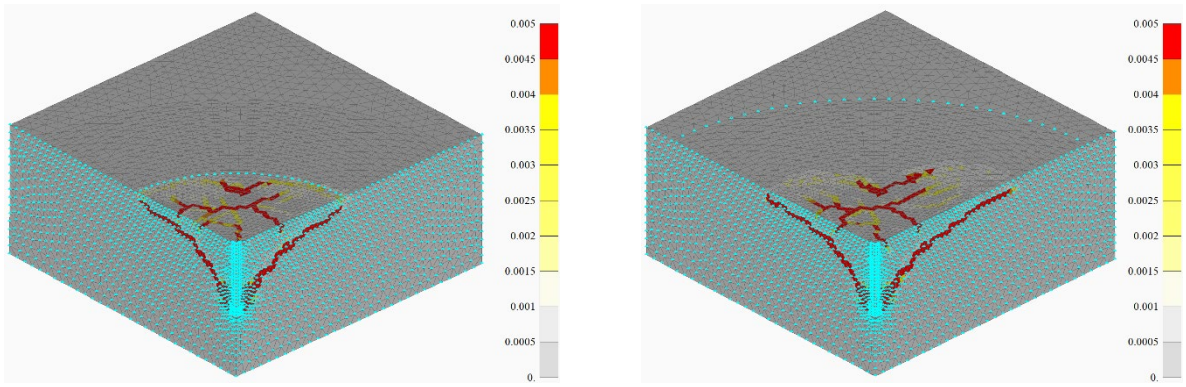

(a) small support ($L_{sup}=4.0h_{ef}$) *(b) large support ($L_{sup}=8.0h_{ef}$)*

Figure 17 – Crack patterns obtained for the headed anchors loaded with small and large supports.

As can be seen, in both cases, anchors fail via concrete cone breakout. It can also be seen that the slop of concrete cone cracks is identical in both cases, albeit the horizontal extension of concrete cone at the concrete surface is slightly larger for the simulated anchor with the large support. Figure 18 also shows the load-displacement relations obtained for the two conditions. As can be seen, the stiffness and capacity of anchors change slightly if the span of vertical support is doubled. From Figs. 17 and 18, it can be concluded that the span of vertical support has negligible influence on the anchorage capacity and the horizontal extension of concrete cone at the concrete surface.

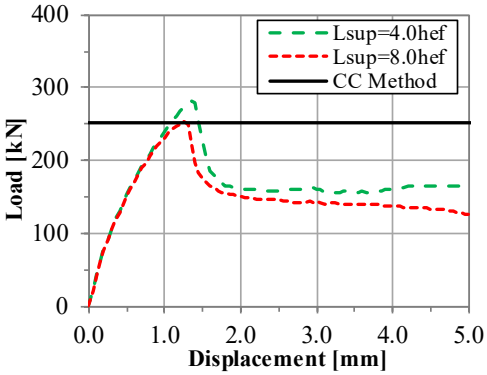

Figure 18 – Numerically obtained load-displacement curves for headed anchors loaded with small and large supports (h_{ef}=200 mm, H=2.0h_{ef})

6. DESIGN PROPOSALS

In this section, the numerical and experimental results at all embedment depths are used to evaluate the reliability of the CC method in predicting the concrete cone failure load of cast-in-place headed anchors. The numerical and experimental results of series a, b, and c showed that the anchorage capacity increases with increase of the member thickness, by enlarging the anchor head size, or if orthogonal surface reinforced is present in the concrete. Taking the influence of these parameters into account can help to improve the prediction accuracy of the failure load of headed anchors with different head sizes in unreinforced and reinforced concrete members of different geometries.

Fig. 19(a) shows ratios of calculated failure loads to the values predicted by the CC method (Eq. 3) as a function of anchor embedment depth for the simulated headed anchors of series (a). As the figure shows, the CC method overestimates the tensile breakout capacity of the short anchors (h_{ef}≤100 mm) in thin unreinforced members, whereas it underestimates the breakout failure load of deep anchors (h_{ef}>100 mm) in thick unreinforced members. This overestimation of the failure load of short anchors is also the case for the modified CC method (Eq. 4), because both equations are identical for short embedment depths (h_{ef} < 280 mm). As previously discussed, this overestimation is attributed to the fact that the tested short anchors that have been considered for the development of the CC method had relatively larger heads and consequently failed at higher loads (than the simulated failure loads in this study).

To account for the overestimation of the failure load of short headed anchors by the CC method and the modified CC method, it is recommended to use the modified CC method (Eq. 4b) regarding large embedment depths (h_{ef}≥ 280 mm) also for small embedment depths as follows:

$$N_{u,m} = 6.585\sqrt{f_c}\,h_{ef}^{5/3} \tag{5}$$

Equation (5) can be used for headed anchors with relatively small heads and embedment depths up to h_{ef}=500 mm in unreinforced concrete members with a member thickness of H=2.0·h_{ef}. The ratios of simulated failure loads of series (a) to the values predicted by Eq. (5) are presented in Fig. 19(b) as a function of anchor embedment depth. As the figure shows, Eq. (5) predicts better the failure load of the simulated headed anchors in relatively thin members, for the entire range of the embedment depths investigated, while still underestimates the anchorage capacity in thick members.

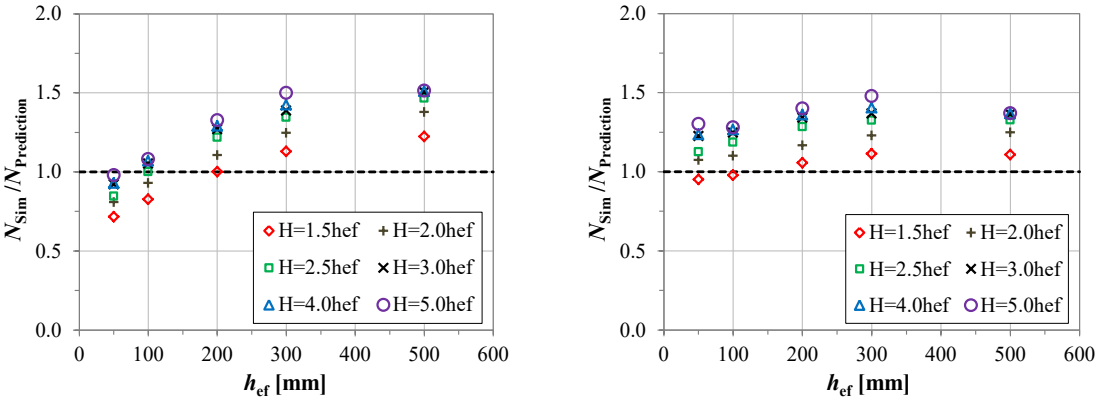

(a) Predictions based on the CC method (Eq. 3) *(b) Predictions based on proposed Eq. (5)*

Figure 19 – Ratio of simulated failure loads to the values predicted by CC method (Eq. 3) and (Eq. 5) as a function of anchor embedment depth for headed anchors in unreinforced concrete members of various thicknesses.

As mentioned before, the failure mode of all the simulated and tested headed anchors in unreinforced concrete members of various thicknesses transitions from concrete splitting to cone breakout failure at a member thickness of H=2.0·h_{ef}. To evaluate the increase rate due to member thickness, all the measured capacities in unreinforced concrete members of various thicknesses, at both tests and simulations, are normalized to the capacity of headed anchors in concrete members with a thickness of (H=2.0·h_{ef}) and plotted in Fig. 20 as a function of the relative member thickness of (H/2.0·h_{ef}). As the figure shows, the relative anchorage capacity increases up to approximately 20% with increasing the relative member thickness. To evaluate the rate of increase in the capacity of headed anchors, two power trend lines were fitted to the test and simulation results. The fitted trend lines coincide and indicate that the relative capacity ($N_{H=1.5\text{-}5.0\cdot hef}/N_{H=2.0\cdot hef}$) at tests and simulations increases proportional to (H/2.0·h_{ef})$^{0.24}$ and (H/2.0·h_{ef})$^{0.25}$, respectively.

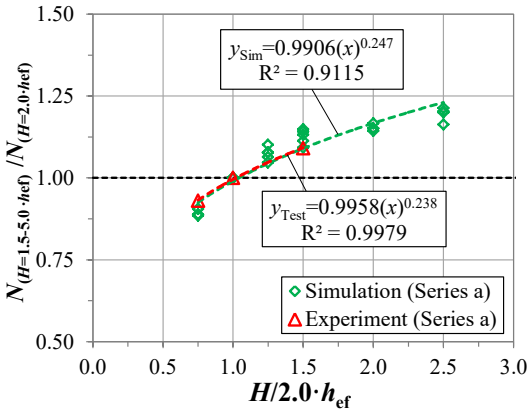

Figure 20 – Relative capacity of tested and simulated anchors in unreinforced concrete members of various thicknesses as a function of relative member thickness.

In the simulation of headed anchors with various head sizes (series b), the concrete pressure (σ_b) under anchor head at peak load for the small-, medium- and large-headed anchors was approximately 20·f_c, 11·f_c, and 4·f_c, respectively. As mentioned before, based on ACI 349 [7] and ACI 318 [8], the mean concrete pressure (σ_b) under the head of a headed anchor in an uncracked concrete member is limited to 15·f_c to prevent a pullout failure. As the concrete pressure of 15·f_c is between the values of concrete pressures under the head of the simulated small- and medium-headed anchors, therefore the minimum required bearing area ($A_{b,min}$), at peak load, was calculated for each embedment depth of anchors using equation below:

$$A_{b,\min} = \frac{N_{u,m}}{15 \cdot f_c} = \frac{16.8\sqrt{f_c}\,(h_{ef})^{1.5}}{15 \cdot f_c} \quad (6)$$

In addition, the capacity of anchors with the minimum required bearing areas ($N_{min.head}$) was estimated by linearly interpolating the calculated capacities of the small- and medium-headed anchors. Fig. 21 shows the relationship between the relative anchorage capacities ($N_{various\ head}/N_{min.head}$) and the relative bearing areas ($A_b/A_{b,min}$) for the simulated and tested headed anchors with various head sizes. As the figure shows, in both tests and simulations, the relative anchorage capacity ($N_{various\ head}/N_{min.head}$) increases by increasing the relative anchor bearing area ($A_b/A_{b,min}$). To evaluate the rate of increase in the capacity of headed anchors with respect to anchor bearing area, two power trend lines were fitted to the test and simulation results. The fitted trend lines indicate that the relative capacity ($N_{various\ head}/N_{min.head}$) at tests and simulations increases proportional to approximately $(A_b/A_{b,min})^{0.13}$ and $(A_b/A_{b,min})^{0.10}$, respectively.

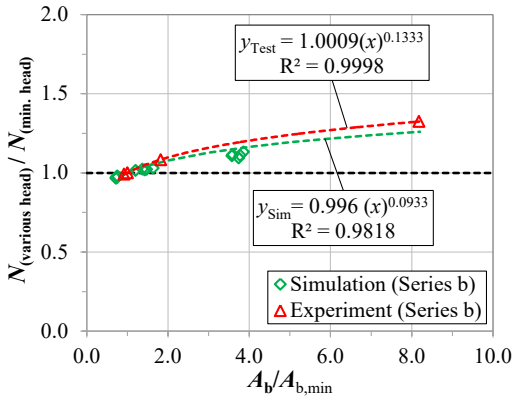

Figure 21 – Relative anchorage capacity as a function of relative anchor bearing area for the simulated and tested headed anchors with different head sizes.

To evaluate the influence of surface reinforcement on the tensile breakout resistance of headed anchors, the relative capacities of tested and simulated headed anchors in reinforced concrete members of various thicknesses (i.e., series c) to the capacity of the corresponding anchors in unreinforced concrete members ($N_{Reinforced}/N_{Unreinforced}$) are plotted in Fig. 22 as a function of a relative member thickness (H/h_{ef}).

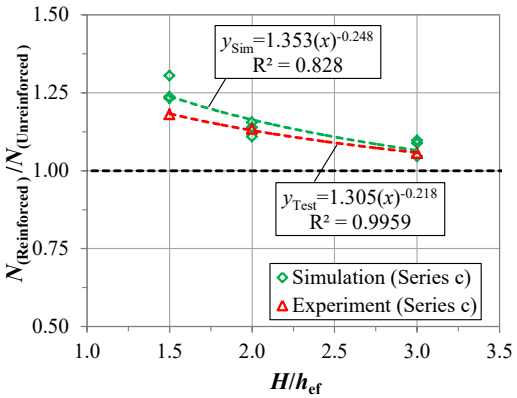

Figure 22 – Relative capacity of anchors in reinforced to unreinforced concrete slabs as a function of relative member thickness (H/h_{ef}) for the simulated and tested headed anchors.

As the figure shows, in both the experiments and simulations, the relative anchorage capacity ($N_{Reinforced}/N_{Unreinforced}$) increases with decrease of the relative member thickness (H/h_{ef}). To evaluate the rate of increase in the capacity of headed anchors, two power trend lines were fitted

to the test and simulation results. The trend lines stipulate that the relative anchorage capacity ($N_{Reinforced}/N_{Unreinforced}$) at test and simulation increases proportional to $[1.31(H/h_{ef})^{-0.22}]$ and $[1.35(H/h_{ef})^{-0.25}]$, respectively.

To account for the influence of member thickness, anchor head size, and surface reinforcement on the capacity of headed anchors, the proposed Eq. (5) is here extended by incorporating three modification factors (namely Ψ_H, Ψ_{AH}, and Ψ_{Sr} respectively for the member thickness, anchor head size, and surface reinforcement) as follows:

$$N_c = N_{u,m} \cdot \psi_H \cdot \psi_{AH} \cdot \psi_{Sr} \tag{7}$$

where Ψ_H, Ψ_{AH}, and Ψ_{Sr} can be calculated as below:

$$\psi_H = \left(\frac{H}{2.0 \cdot h_{ef}} \right)^{0.25} \leq 1.20 \tag{8}$$

$$\psi_{AH} = \left(\frac{A_b}{A_{b,min}} \right)^{0.1} \tag{9}$$

$$\psi_{Sr} = \begin{cases} 1.35\left(\frac{h_{ef}}{H} \right)^{0.25} \leq 1.20 & \text{for } H \leq 3.0 \cdot h_{ef} \\ 1.00 & \text{for } H > 3.0 \cdot h_{ef} \end{cases} \tag{10}$$

where H: member thickness [mm], h_{ef}: anchor embedment depth [mm], A_b: anchor bearing area [mm^2], and $A_{b,min}$: the minimum required bearing area corresponding to a concrete pressure (σ_b) of $15 \cdot f_c$ under anchor head at peak load which can be determined from Eq. (6).

The proposed modification factor Ψ_H was extracted from Fig. 20. Ψ_H is limited to 1.20 as it was found that the tensile capacity of headed anchors increases up to approximately 20% with increasing the member thickness. The simulation results of series (a) revealed that, for Ψ_H<1.0, unreinforced concrete members fail by concrete bending/splitting, whereas for $\Psi_H \geq 1.0$ both reinforced and unreinforced concrete members fail via concrete cone breakout. The proposed Eq. (7) can predict the failure load associated with both the concrete cone and concrete splitting failure modes of headed anchors. Compared to the CC method, Eq. (7) is more conservative as it gives a lower failure load for the headed anchors in relatively thin unreinforced concrete members (H<2.0·h_{ef}). For design of headed anchors, one need also to calculate the bending cracking failure load of the concrete component, based on the theory of elasticity or yield line theory, and compare it with the failure load predicted by Eq. (7). It would be obvious that the lowest failure load will govern the anchorage.

The proposed modification factor Ψ_{AH} was extracted from Fig. 21. Ψ_{AH} is smaller than one for anchors with small heads (when anchor bearing area A_b is smaller than the minimum required bearing area $A_{b,min}$) and thus, compared to the CC method, Eq. (7) predicts lower failure loads for headed anchors with the small heads. Based on the numerical and experimental results, it was realized that the average concrete cone angle with respect to the concrete surface decreases with increasing head size. In the case of anchors with large heads, the diameter of the concrete cone at the concrete surface is >4.0·h_{ef}. This differs from the projected failure area of (3.0·h_{ef} × 3.0·h_{ef}) assumed by the CC method. Currently, the characteristic anchor spacing (s_{cr}) for a group of headed

anchors and edge distance (c_{cr}) for headed anchors close to free concrete edges is limited to $3.0 \cdot h_{ef}$ and $1.5 \cdot h_{ef}$, respectively [4-8]. If the concrete cone envelope obtained for the tested and simulated large-headed anchors in this study is extended to reach the concrete surface, the diameter of the concrete cone at the concrete surface is approximately $5.0 \cdot h_{ef}$. Therefore, for the design of headed anchors with large heads in groups or close to concrete free edges, the characteristic anchor spacing (s_{cr}) and the characteristic edge distance (c_{cr}) should be increased to $5.0 \cdot h_{ef}$ and $2.5 \cdot h_{ef}$, respectively.

The proposed modification factor Ψ_{Sr} was also extracted from Fig. 22. Ψ_{Sr} is also limited to 1.20 as the numerical and experimental results showed an increase of up to approximately 20% in the capacity of headed anchors if orthogonal surface reinforcement is present. It was also shown that the favorable influence of surface reinforcement on the anchorage capacity decreases by increasing the thickness of the concrete component. It should be noted that the proposed Ψ_{Sr} factor is applicable if the concrete member is orthogonally reinforced with a minimum reinforcement content of ($\rho \approx 0.3\%$) in each direction.

To further evaluate the validity of the proposed model (Eq. 7) in predicting the capacity of single headed anchors with various head sizes in plain and reinforce concrete members of various thicknesses, the failure load of 124 pullout tests on single headed anchors from literature and those tests in the test series (a, b, and c) in this study are compiled in the following and compared with the corresponding values predicted by the CC method and the proposed model. The experimental data from literature were previously reported by Eligehausen et al. [10], Nilsson et al. [11], Zhao [12], and Lee et al. [13]. As in these studies, the concrete compressive strength, the thickness of concrete component, the size of anchor head, and the amount of orthogonal surface reinforcement were variable, all measured capacities were normalized and presented in Fig. 23 as a function of anchor embedment depth. In these experiments, headed anchors at various embedment depths (up to h_{ef}=1143 mm) were tested in concrete slabs of different strengths. Since the concrete strength at different tests was measured on concrete cube or cylinder specimens, all the measured concrete cube compressive strengths at tests were initially converted to their equivalent cylinder compressive strengths using the following relation ($f_c \approx 0.84 \cdot f_{cc}$). The measured concrete cylinder compressive strengths at tests vary from 19.1 to 45.1 [N/mm^2]. All the measured failure loads at tests were then normalized to a concrete cylinder compressive strength of f_c=28 [N/mm^2] using a normalizing factor of $(28/f_{c,test})^{0.5}$.

In addition, the tested headed anchors were in concrete members of different thicknesses. The relative member thickness ($H/2.0 \cdot h_{ef}$) for the tested anchors varies from 0.57 to 1.65. Therefore, all the measured failure loads at tests were further normalized to a relative member thickness of ($H/2.0 \cdot h_{ef}$=1) using a normalizing factor of $[1/(H/2.0 \cdot h_{ef})_{test}]^{0.25}$. Moreover, the relative bearing area ($A_b/A_{b,min}$) of tested headed anchors varies from approximately 0.8 to 8.1. Therefore, all failure loads at tests were further normalized to a relative bearing area of ($A_b/A_{b,min}$=4.0) using a normalizing factor of $[4/(A_b/A_{b,min})_{test}]^{0.1}$. The applied normalizing factors are based on the proposed model (Eq. 7), as stipulates that the tensile breakout capacity is proportional to $(f_c)^{0.5}$, $(H/2.0 \cdot h_{ef})^{0.25}$, and $(A_b/A_{b,min})^{0.1}$. Furthermore, the reinforcement-content of the tested concrete slabs varies from 0% to 1.16%. As the proposed model (Eq. 7) stipulates different values for the modification factor Ψ_{Sr} depending on the member thickness, therefore the value of Ψ_{Sr} was evaluated for all tested concrete slabs and then all the measured failure loads at tests were further normalized to Ψ_{Sr}=1.0 using a normalizing factor of $[(1/(\Psi_{sr})_{test}]$.

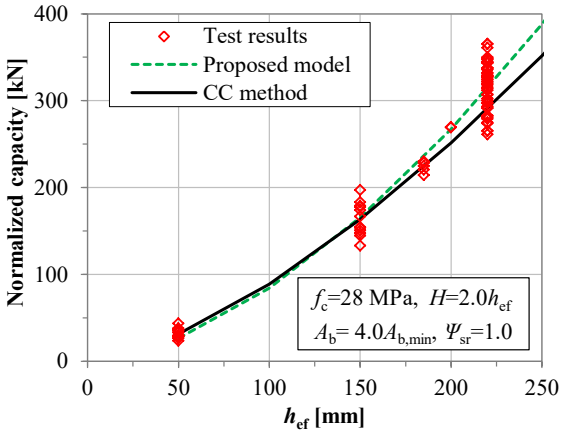

(a) for h_{ef} up to 220 mm

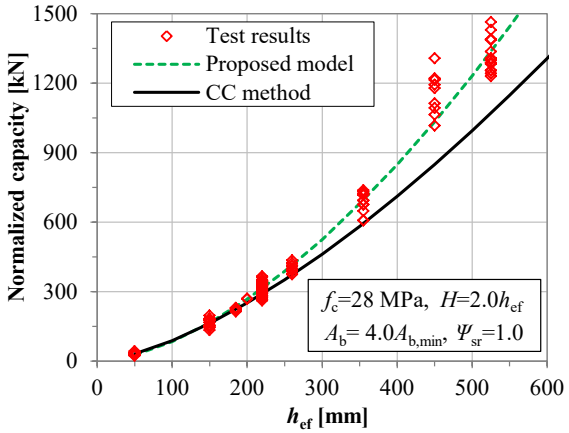

(b) for h_{ef} up to 530 mm

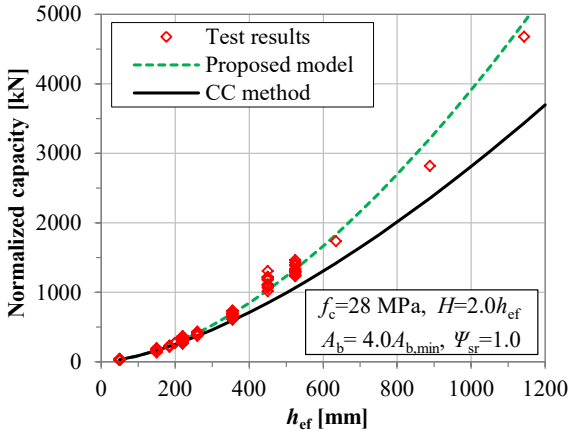

(c) for h_{ef} up to 1143 mm

Figure 23 – Normalized concrete cone failure load of the tested anchors in this study and 124 anchors from literature [10-13] as a function of embedment depth; comparison between measured capacities at tests and predictions via the CC method (Eq. 3) and the proposed model (Eq. 7).

Figure 23 also shows the normalized failure loads predicted by the CC method and the proposed model (Eq. 7). As the figure shows, the CC method (Eq. 4) underestimates the tensile breakout capacities of deep anchors. In contrast, the proposed model (Eq. 7) better predicts the normalized capacity of the tested anchors for the embedment depths up to 635 mm. However, it seems that the proposed model (Eq. 7) overestimates slightly the anchorage capacity of anchors with embedment depths>635 mm. There are two possible reasons for this overestimation: (*a*) the reported concrete compressive strengths for the tested deep anchors (h_{ef}≥635 mm) were measured on small cylinder specimens, whereby the tested anchorage components were extremely large, and their mechanical properties could have been possibly reduced due to the effect of non-elastic deformations (i.e., creep, shrinkage, temperature, etc.). Therefore, the measured strengths in the experiments with h_{ef}≥635 mm may not necessarily represent the actual strength of tested anchorage components. (*b*) The tests on deep headed anchors reported by Lee et al [13] were performed in concrete components with different geometrical conditions than those considered in the numerical and experimental studies presented in the current paper. Indeed, the width of concrete components in the tests with h_{ef}≥635 mm was (3.6-5.0)·h_{ef}, while it was 6.0·h_{ef} in the conducted numerical and experimental studies presented in this paper. As the tested headed anchors with h_{ef}≥635 mm had quite large heads, their failure cone fracture could have not been fully developed, due to possible truncation of the concrete cone fracture with the concrete free edges. The truncated concrete cone envelope may theoretically result in reduced capacities for

these anchors. In fact, the capacity of the tested anchors could have been higher if they had been tested in wider concrete components.

Nevertheless, to ensure the accuracy of the proposed model in predicting the capacity of headed anchors with embedment depths >635 mm, further experimental and numerical evaluations of deep headed anchors are required. Until the result of these evaluations become available, it is recommended to use the proposed model (Eq. 7) for the maximum embedment depths given in ACI 349 [7] and ACI 318 [8] only (i.e., $h_{ef} \leq 635$ mm).

6. CONCLUSIONS

The influence of the thickness of concrete member, size of anchor head, and amount of orthogonal surface reinforcement on the concrete-related failure load of tension loaded headed anchors was evaluated both numerically and experimentally. Based on the experimental and numerical results, it was found that the ultimate capacity of headed anchors increases by increasing member thickness or if a small amount of orthogonal surface reinforcement ($\rho \approx 0.3\%$ in each direction) is present at the anchoring zone. Furthermore, the anchorage post-peak resistance increases when orthogonal surface reinforcement is present. This is attributed to an increase of the global bending stiffness of the concrete members which is obtained by increasing the member thickness or adding surface reinforcement.

The anchorage fails by concrete splitting in relatively thin unreinforced concrete ($H<2.0h_{ef}$). However, a small amount of orthogonal surface reinforcement can prevent concrete splitting failure and change the failure mode to concrete cone breakout, thereby increasing the anchorage capacity. It was also found that the increase rate due to surface reinforcement is dependent on the member thickness: the thinner the concrete member the larger the favorable influence of surface reinforcement on the anchorage capacity. The numerical results further showed that a large-reinforcement ratio does not improve the tensile capacity and performance of headed anchors any further than what a small-reinforcement ratio does.

Both the tests and simulations showed that the tensile breakout capacity of headed anchors further increases by increasing the bearing area of anchors' head. However, the anchorage behavior becomes stiffer and more brittle when enlarging the head size. In the current standards, the characteristic anchor spacing (s_{cr}) for a group of anchors and edge distance (c_{cr}) for anchors close to concrete free edge/s are considered as $3.0 \cdot h_{ef}$ and $1.5 \cdot h_{ef}$, respectively. Both the numerical and experimental results showed that the average cone angle with respect to the concrete surface decreases with increase of head size. In the case of anchors with large heads, the diameter of the concrete cone at the concrete surface was $>4.0 \cdot h_{ef}$. This differs from the projected concrete cone failure area of $(3.0 \cdot h_{ef} \times 3.0 \cdot h_{ef})$ on the concrete surface, assumed by the CC method. Therefore, for the design of anchors with large heads in groups or close to concrete free edge/s, it is recommended to increase s_{cr} and c_{cr} to $5.0 \cdot h_{ef}$ and $2.5 \cdot h_{ef}$, respectively.

It was demonstrated that the CC method overestimates the capacity of short anchors ($h_{ef} \leq 100$ mm) if anchors have relatively small heads or positioned in relatively thin unreinforced concrete members. It was, on the other hand, realized that the CC method underestimates the tensile capacity of deep anchors if they have large heads or positioned in relatively thick members. To refine the CC method and better predict the tensile breakout capacity of cast-in-place headed anchors with various head sizes in unreinforced and reinforced uncracked concrete members of various thicknesses, the CC method (Eq. 3) was modified and further extended, see Eq. (7), by

incorporating three modification factors to take the influence of member thickness, anchor head size, and orthogonal surface reinforcement into account.

The proposed Eq. (7) should be used only for the maximum embedment depths given in ACI 349 [7] and ACI 318 [8] (i.e., $h_{ef} \leq 635$ mm). To extend the application of Eq. (7) to headed anchors with $h_{ef} > 635$ mm, further numerical and experimental evaluations of headed anchors at larger embedment depths (than considered in this study) are required.

REFERENCES

1. Eligehausen R, Mallée R & Silva J F: "Anchorage in Concrete Construction". Ernst & Sohn, Berlin, Germany, 2006, 378 pp.
2. ACI Committee 349: "Code Requirements for Nuclear Safety-Related Concrete Structures (ACI 349-85)". American Concrete Institute, Detroit, USA, 1985.
3. Fuchs W, Eligehausen R & Breen J E: "Concrete Capacity Design (CCD) Approach for Fastening to Concrete". *ACI Structural Journal*, Vol. 92, No. 1, 1995, pp. 73–94.
4. CEB: "Design of Fastenings in Concrete, Comité Euro-International du Béton". Thomas Telford, Lausanne, Switzerland, 1997, 92 pp.
5. CEN/TS 1992-4: "CEN Technical Specification (TS): Design of Fastenings for Use in Concrete, Final Draft". European Organization for Standardization (CEN), Brussels, Belgium, 2009, 166 pp.
6. *fib* Bulletin 58. "Design of Anchorages in concrete – Guide to good practice". International Federation for Structural Concrete, Lausanne, Switzerland, 2011, 280 pp.
7. ACI 349: "Code Requirements for Nuclear Safety-Related Concrete Structures, Appendix D". American Concrete Institute, Farmington Hills, MI, USA, 2006.
8. ACI 318: "Building Code Requirements for Structural Concrete and Commentary". American Concrete Institute, Farmington Hills, MI, USA, 2014, 524 pp.
9. Ožbolt J, Eligehausen R, Periškić G & Mayer U: "3D FE Analysis of Anchor Bolts with Large Embedment Depths," *Engineering Fracture Mechanics*, Vol. 74, Nos. 1-2, 2007, pp.168-178.
10. Eligehausen R, Bouška P, Červenka V & Pukl, R: "Size Effect of the Concrete Cone Failure Load of Anchor Bolts". *Proceedings*, 1st International Conference of Fracture Mechanics of Concrete Structures (FRAMCOS 1), Z.P. Bazant, ed., 1992, pp. 517–525.
11. Nilsson M, Ohlsson U & Elfgren L: "Effects of Surface Reinforcement on Bearing Capacity of Concrete with Anchor Bolts." *Nordic Concrete Research*, No. 44, 2011, pp. 161–174.
12. Zhao G: "Tragverhalten von randfernen Kopfbolzenverankerungen bei Betonbruch". *Ph.D. Dissertation*, University of Stuttgart, Stuttgart, Germany, 1993, 204 pp. (In German).
13. Lee, N. H., Kim, K. S., Bang, C. J., & Park, K. R., (2007). "Tensile-headed anchors with large diameter and deep embedment in concrete". *ACI Structural Journal*, Vol. 104, No. 4, 2007, pp. 479-486.
14. Ožbolt J, Li Y & Kožar I: "Microplane Model for Concrete with Relaxed Kinematic Constraint," *International Journal of Solids and Structures,* Vol. 38, No. 16, 2001, pp. 2683-2711.
15. Bažant Z P & Oh B H: "Crack Band Theory for Fracture of Concrete," *Materials and Structures (RILEM)*, Vol. 16, No. 3, 1983, pp. 155-177.

16. Nilforoush R: “Anchorage in Concrete Structures: Numerical and Experimental Evaluations of Load-Carrying Capacity of Cast-in-Place Headed Anchors and Post-Installed Adhesive Anchors”. *Ph.D. Dissertation*, Dep. of Civil, Environment and Natural Resources Engineering, Div. of Structural and Fire Engineering, Luleå University of Technology, Luleå, Sweden, 2017, 354 pp.
17. EN 12390-3 (2009). “Testing hardened concrete. Compressive strength of test specimens”. 19 pp.
18. EN 12390-6 (2009). “Testing hardened concrete. Tensile splitting strength of test specimens”. 11 pp.
19. Nilforoush R, Nilsson M, Elfgren L, Ožbolt J, Hofmann J & Eligehausen, R: “Tensile Capacity of Anchor Bolts in Uncracked Concrete: Influence of Member Thickness and Anchor’s Head Size”. *ACI Structural Journal,* Vol. 114, No. 6, 2017, pp. 1519-1530
20. Nilforoush R, Nilsson M, Elfgren L, Ožbolt J, Hofmann J & Eligehausen R: “Influence of Surface Reinforcement, Member Thickness, and Cracked Concrete on Tensile Capacity of Anchor Bolts”. *ACI Structural Journal,* Vol. 114, No. 6, 2017, pp. 1543-1556
21. Nilforoush, R., Nilsson, M., Elfgren, L., “Experimental Evaluation of Influence of Member Thickness, Anchor-Head Size, and Reinforcement on the Tensile Capacity of Headed Anchors in Uncracked Concrete”, *Journal of Structural Engineering*, Vol. 144, No. 4, 2018, 14 pp, 04018012-1-14.